

Cure monitoring of fibre reinforced composites using infrared imaging and data assimilation

by Gernot Mayr*, Guenther Mayr* and Gerald Zauner*

* Research Group of Thermography & NDT, University of Applied Sciences Upper Austria, School of Engineering, Wels, Austria

Abstract

A passive monitoring system using infrared imaging and thermal measurements was developed to predict the degree of cure in fiber-reinforced polymer composites. Using an Ensemble Kalman Filter approach finite element simulations and thermal measurements are combined to estimate the degree of cure in-situ. It was tested on carbon-fibre-reinforced-plastic (CFRP) samples in an industrial oven and the results are comparable to a dielectric sensor. The system can be extended to complex parts and allows the addition of more thermal sensors or the incorporation of other curing sensors.

1. Introduction

Production of fiber-reinforced polymer (FRP) composites using thermosetting polymers necessitates heating of these parts in industrial autoclaves. In-situ monitoring this process can reduce the environmental impact, as it allows the optimisation of the process and the efficient utilisation of resources. Thermosetting polymers are used in various industries either in pure form or as a matrix material in composite materials. For instance, thermosetting polymers in form of resins are used as coatings for components or for the impregnation of fibre bundles or woven fabric. Resins are viscous to soft substances containing prepolymers or monomers with reactive groups. By increasing the energy in the resin, for example, by increasing the resin temperature or by stimulation with light, chemical reactions are triggered. These reactions transform the resin into a solid state. This irreversible polymerisation process, known as curing, turns the prepolymers into an infusible, insoluble polymer network[1]. The reaction of thermosets is modelled with reaction equations, which are in general autonomous ordinary differential equations of the form

$$\frac{d}{dt}\xi(t) = f(T(t), \xi(t)) \quad (1)$$

with ξ as the degree of cure (DoC) and a nonlinear, temperature- and DoC-dependent function f . Usually f incorporates the Arrhenius equation, i.e. with increasing temperature T the rate of reaction increases as well. Once the parameters of Eq. (1) are determined experimentally, it allows the estimation of the DoC with different temperature profiles (see Fig. 1). FRP-composites using thermosetting polymers are often cured in large industrial autoclaves with an inhomogeneous temperature distribution inside the autoclave. Especially for thick composites, a estimation of the DoC based on an a-priori temperature is not representative for the actual DoC. When a certain DoC must be reached to ensure the part quality, a significant safety margins with respect to the curing time is necessary. Therefore, the more accurate the real temperature inside the part is known, the better the DoC estimation based on Eq. (1) will be.

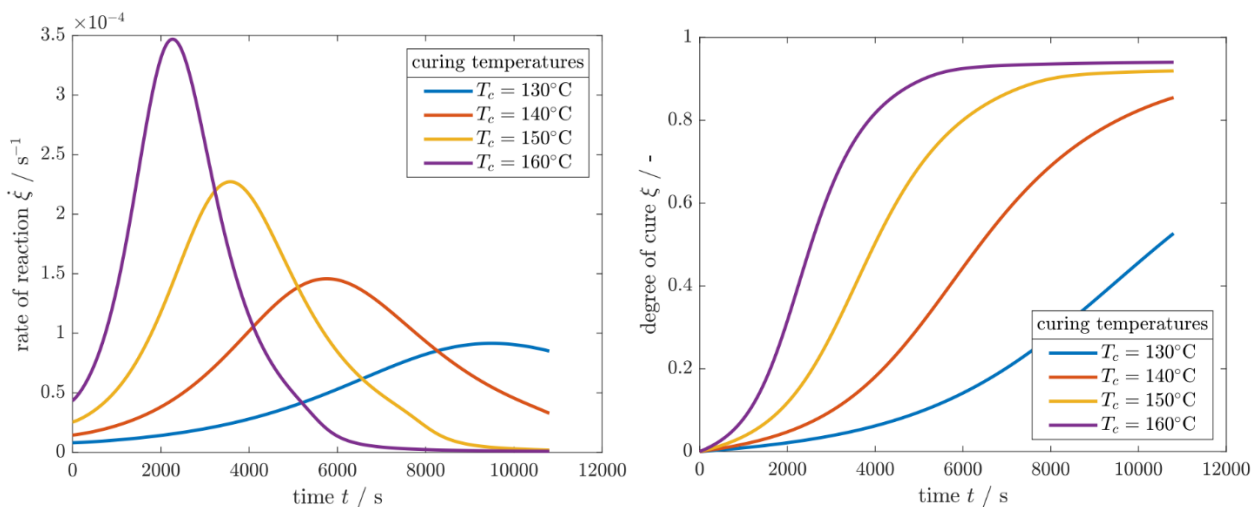


Fig. 1. Example of a thermosetting polymer reaction at different isothermal curing temperatures

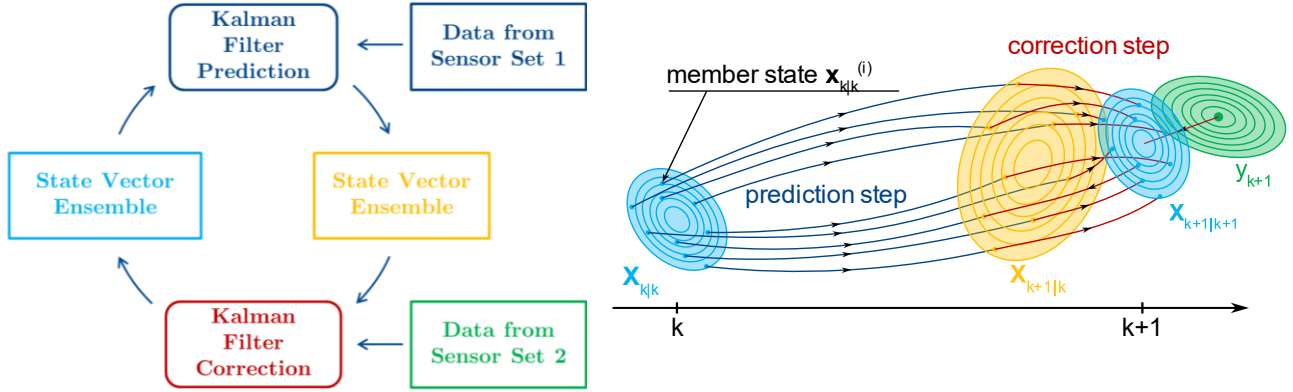


Fig. 2. Principles of the EnKF: cyclic prediction and correction (left graphic) and the propagation of the ensemble in discrete time steps (right graphic, modified from [2])

With data assimilation (DA) methodologies, large and non-linear dynamic models can be combined with observations [3]. The goal is to enhance the accuracy of the model by modifying the state or the parameters of the model. In this work the Ensemble Kalman Filter (EnKF) method developed by Evensen [4] is adapted. The principle idea is shown in Fig. 2. Unlike the classic Kalman Filter (KF), which uses the entire state distribution explicitly as a covariance matrix to describe the model errors, the EnKF is a sequential Monte Carlo method that uses an ensemble of states to approximate the distribution of the state [5, 6]. This makes the EnKF feasible for large state vectors and allows the parallelisation of the prediction step [7]. The ensemble is corrected when new observations become available. While non-linear models can be used for the prediction and to transform observations to state variables, the correction step is still based on a linear state space model like the classic KF [8]. The EnKF has been utilised to estimate the internal temperature and the thermal conductivity distribution during the curing of a carbon-fibre-reinforced polymer (CFRP) [9]. Using an EnKF, the thermal conductivity of cast iron and the heat transfer coefficient between melt and alloy of this material was estimated [10].

Thermography has a wide range of applications in the field of active and passive imaging. In the context of DoC prediction however, it has been considered only in numerical studies, e.g. for the estimation of the generated curing heat of CFRP [11]. There, the heat transfer coefficients of convection and heating were estimated as well.

In the presented work, an approach to simultaneously estimate the internal temperature and the DoC of CFRP parts using an EnKF is presented. The developed system combines infrared camera images with thermocouple data and a thermochemical model.

2. Methods

2.1. Implementation of the Ensemble Kalman Filter

The EnKF iteration scheme was implemented according to [8]. The state vector \mathbf{x}_k at the time step k is corresponding to N nodes of the FEM model which also includes the nodes for the surface of the bagging. In addition, the state is augmented by tool and air temperatures and the degree of cure ξ for I internal nodes belonging to the part:

$$\mathbf{x}_k = [T_k^1 \dots T_k^n \dots T_k^N \quad T_k^{tool} \quad T_k^{bgr} \quad \xi_k^1 \dots \xi_k^i \dots \xi_k^I]^T. \quad (2)$$

The measurement vector is

$$\mathbf{y}_k = [\hat{T}_k^{r,1} \dots \hat{T}_k^{r,s} \dots \hat{T}_k^{r,S} \quad \hat{T}_k^{tool} \quad \hat{T}_k^{bgr}]^T \quad (3)$$

and contains the camera raw data $\hat{T}_k^{r,s}$ interpolated to S surface nodes as well as the tool and air temperatures. The prediction step is the simulation of M independent ensemble members $\mathbf{x}_{k+1|k}^{(i)}$ from step k to $k+1$ resulting in a prediction ensemble

$$\mathbf{X}_{k+1|k} = \{\mathbf{x}_{k+1|k}^{(i)}\}_{i=1}^M = g(\mathbf{X}_{k|k}) + \mathbf{V}_k. \quad (4)$$

g represents the thermal simulation with the initial conditions $\mathbf{X}_{k|k}$, which denotes the ensemble from the previous correction step. \mathbf{V}_k is an ensemble of M independent process noise realizations $\{\mathbf{v}_k^{(i)}\}_{i=1}^M$ with zero mean and covariance \mathbf{Q} . The predicted measurements ensemble is

$$\mathbf{Y}_{k+1|k} = \{\mathbf{y}_{k+1|k}^{(i)}\}_{i=1}^M = h(\mathbf{X}_{k+1|k}) + \mathbf{E}_k. \quad (5)$$

Here the function h describes the relation between the state and the observed variables. In our case a background correction is implemented that corrects the thermal image data. \mathbf{E}_k is a matrix with artificial zero-mean measurement noise realizations $\{\mathbf{e}_k^{(i)}\}_{i=1}^M$ with covariance \mathbf{R} . The Kalman Gain $\bar{\mathbf{K}}_k$ is a weighting matrix for the error between predictions and observations and is

$$\bar{K}_k = (\tilde{X}_{k+1|k} \tilde{Y}_{k+1|k}^T) (\tilde{Y}_{k+1|k} \tilde{Y}_{k+1|k}^T)^{-1}. \quad (6)$$

It can be calculated using the ensembles of deviations

$$\tilde{X}_{k+1|k} = X_{k+1|k} \left(\mathbf{I}_V - \frac{1}{V} \mathbb{1}_V \mathbb{1}_V^T \right) \quad (7)$$

$$\tilde{Y}_{k+1|k} = Y_{k+1|k} \left(\mathbf{I}_W - \frac{1}{W} \mathbb{1}_W \mathbb{1}_W^T \right) \quad (8)$$

where \mathbf{I}_i is the identity matrix of size i and $\mathbb{1}_i^T = [1 \dots 1]$ is an i -dimensional vector. The subscripts V and W are the total sizes of the state and observation vectors. The update equation is

$$X_{k+1|k+1} = X_{k+1|k} + \bar{K}_k (\hat{y}_k \mathbb{1}_W^T - Y_{k+1|k}) \quad (9)$$

which is identified with $X_{k|k}$ for the next iteration. The prediction steps for each member are computed in parallel and the correction step is carried out as soon as all simulations are finished. It is assumed that computing the DoC for each member will not increase the accuracy. Therefore, the mean state vectors $\bar{x}_k = \frac{1}{V} X_{k|k} \mathbb{1}_V$ and $\bar{x}_{k+1} = \frac{1}{V} X_{k+1|k+1} \mathbb{1}_V$ as well as ξ_k^i as initial conditions are used for computing ξ_{k+1}^i .

2.2. Dynamic Prediction Model

For the prediction step the finite element analysis (FEA) is used to compute the thermal behavior during curing. The model, as outlined in Fig. 3, consists of the part to be cured, the bagging and the tool and is therefore a simplification of the real thermal problem. For the anisotropic CFRP domain the heat conduction equation is

$$c_p \rho \frac{\partial}{\partial t} T(t) - \frac{\partial}{\partial x} \left(k_{xx} \frac{\partial}{\partial x} T(t) \right) - \frac{\partial}{\partial y} \left(k_{yy} \frac{\partial}{\partial y} T(t) \right) - \frac{\partial}{\partial z} \left(k_{zz} \frac{\partial}{\partial z} T(t) \right) = \rho_R V_R H_r \frac{\partial}{\partial t} \xi(t, x, y, z) \quad (10)$$

and includes a volumetric heat source term for the exothermal reaction, which is proportional to the rate of reaction $\frac{\partial}{\partial t} \xi$. ρ_R is the resin density, V_R is the volumetric fraction of the resin matrix (40%) and H_r is the total heat of reaction of the resin. c_p , ρ and k are the specific heat capacity, density and thermal conductivities of the composite. Furthermore, only the surface breather is modeled instead of all layers the vacuum bagging actually consists of. This is reasonable as the influence of release films, vacuum bag etc. are negligible compared to the breather material. It is a porous polyamide (PA) foam and modelled with effective material properties containing 1 wt.% air. Relevant model parameters can be found in Table 1. As a simplification, the material parameters are kept constant. Values of the cured material were used under the assumption that the estimation of the thermal distribution in later stages of the curing will be more accurate. The environment around the sample (air and oven) is considered by convective and radiating boundary conditions only. The temperature solution is obtained using Quadratic Lagrange shape functions for the discretization.

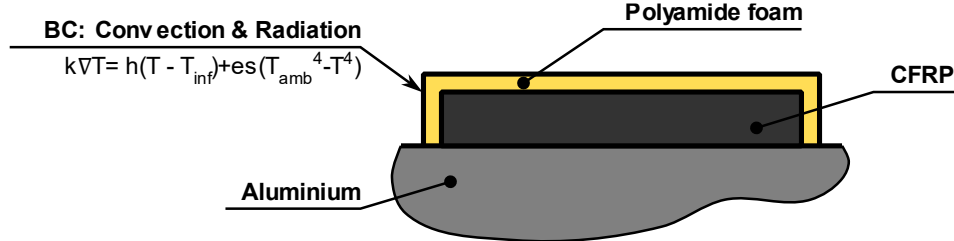


Fig. 3. Cross section of the dynamic model

Table 1. Relevant material parameters for the dynamic model

Parameter	Unit	CFRP	Aluminium	PA foam
In-plane thermal conductivity	W/(m K)	1.28	238	0.026
Out-of-plane thermal conductivity	W/(m K)	0.64	238	0.026
Density	kg/m ³	1600	2700	77.7
Specific heat capacity	J/(kg·K)	1200	900	709.6
Thickness	mm	2	5	1

For the computation of the degree of cure based on the thermal history, the parameters of the kinetic equation must be identified. The material was characterized in accordance to [12] using dynamic scanning calorimetry (DSC), i.e. Eq. (1) is adapted to a model with two independent kinetic equations:

$$\frac{d}{dt} \xi_1(t) = A_1 \exp\left(-\frac{E_{a1}}{RT}\right) \xi_1(t)^{m_1} (1 - \xi_1(t))^{n_1} \quad (11)$$

$$\frac{d}{dt} \xi_2(t) = A_2 \exp\left(-\frac{E_{a2}}{RT}\right) \xi_2(t)^{m_2} (1 - \xi_2(t))^{n_2} \quad (12)$$

$$\frac{d}{dt} \xi(t) = r_1 \frac{d}{dt} \xi_1(t) + (1 - r_1) \frac{d}{dt} \xi_2(t). \quad (13)$$

Based on several independent isothermal heating & dynamic heating experiments the identified material properties were estimated (see Table 2). The prepreg material is plain weave CFRP with epoxy matrix (CYCOM® 970). The recommended cure cycle is two hours at 177°C and is suitable for autoclave processing. Eq. (11)-(13)(12) are solved only for the CFRP material domain of the model. The solution is obtained using Linear Lagrange shape functions for the discretization.

The temporal step width for the thermal as well as for the kinetic model is 1 min. That is, an ahead prediction of 1 min is performed. Afterwards, the node temperature and DoC values are extracted from the model and used as the state prediction in the EnKF. As soon as the correction step is finished, the new state is used as an initial condition for the next time step in the FEA model. For each member a model instance is kept in the computer memory, allowing to compute predictions of the ensemble members in parallel, i.e. $x_{k+1|k}^{(i)}$ and $y_{k+1|k}^{(i)}$ in Eq. (4)–(5). Once every instance is finished with the computation, the correction step, Eq. (6)–(9), is carried out. The state x_k contains 929 node temperatures and 478 node DoC values and depends on the finite element mesh that is created (here tetrahedral elements were used). All the simplifications described above result in a model error. This uncertainty can be controlled by the matrix V_k in the prediction step of the EnKF. The number of ensemble members is limited to 20 in order to keep the computation time shorter than the temporal step width.

Table 2. Estimated parameters for the cure model

Parameter	Unit	Reaction 1	Reaction 2
A_i	1/s	1.080e7	9.130e7
m_i	1	0.308	0.625
n_i	1	1.700	0.980
$E_{a,i}$	J/mol	82.48e3	93.31e3
r_i	1	0.83	0.17
$\Delta H_{0,i}$	J/kg	499.00e3	99.50e3

2.3. Experimental setup

An overview of the setup is depicted in Fig. 4 and a picture Fig. 5. The thermal radiation emitted by the sample is acquired with an infrared camera, which can be used to measure the surface temperature of the sample. In the context of DA, each camera pixel represents a sensor which provides thermal data in regular time intervals. The microbolometer camera Optris PI640i (field of view 60°x45°, resolution 640 x 480 px, NETD 40 mK, max. framerate 60 Hz) is used. To keep the camera within its allowed operational conditions it is placed inside of a water-cooled housing. The optical window is transparent for radiation in the long-wave range where also the detector of the camera has its highest sensitivity (8 – 14 μm).

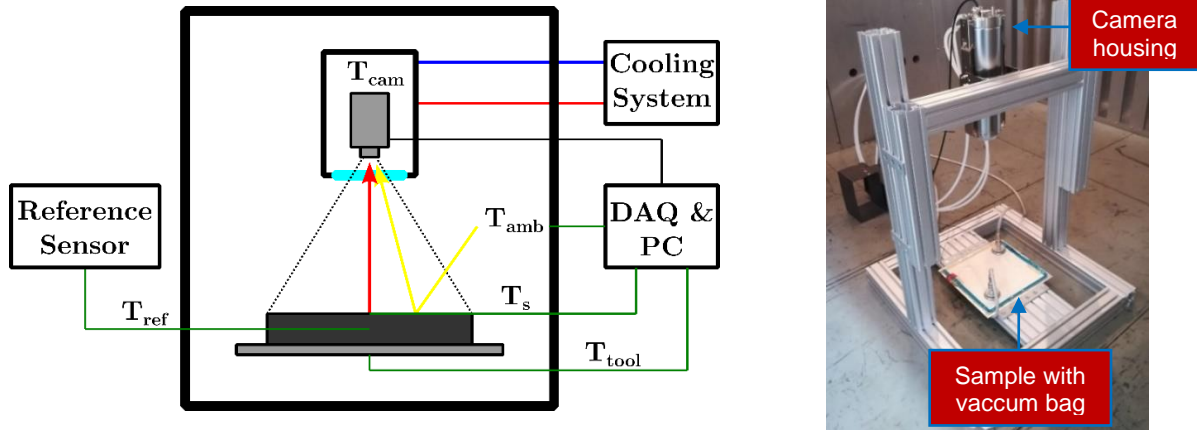


Fig. 4. Principle overview of the experimental setup (left) and a picture of the setup in the industrial oven (right)

Neglecting thermal radiation from the air and assuming a homogenous wall temperature, the thermal radiation collected by the camera can be approximated with a combination of the actual surface temperature and the ambient temperature:

$$f_c(T_s, T_{amb}) = \varepsilon \frac{R}{\exp\left(\frac{B}{T_s}\right) + F} + (1 - \varepsilon) \frac{R}{\exp\left(\frac{B}{T_{amb}}\right) + F}. \quad (14)$$

Since the camera is calibrated providing absolute temperature data and an optical window is in the optical path, the function $f_c(T_s, T_{amb})$ includes apparent parameters. These parameters were estimated using several independent experiments where thermocouples were used to measure the ambient temperature and the surface temperature over a temperature range of 20 °C – 185 °C (results see Table 3). Eq. (14) can be directly integrated in the EnKF, i.e. in Eq. (5) the

measurement function is $h = [f_c(T_k^s, T_k^{amb}) \dots f_c(T_k^s, T_k^{amb}) \dots f_c(T_k^s, T_k^{amb}) \ T_k^{tool} \ T_k^{amb}]^T$. The camera image is linear interpolated to match the measurement data with the node coordinates on the surface of the simulation model.

Table 3. Estimated parameters for the correction function Eq. (14)

Parameter	Unit	R ² =0.99
ε	1	0.808
R	°C	11.370
B	°C	9.233
F	1	0.989

To validate the EnKF results, a dielectric sensor is used which can be seen in Fig. 5. The principles of this method can be found in [13]. In this sensor a small single layer CFRP sample is cured in a heating chamber under the same thermal conditions as the real part. For this, the temperature inside the chamber is controlled by measuring the temperature with a thermocouple which is placed inside the part in the oven. The reference sensor measures the DC-resistance of the sample which is related to the ion viscosity of the resin. This physical property is highly temperature dependent, thus the compensation function [14]

$$\xi_{ref} = \frac{c_{0,0} + c_{1,0}T - \log(R)}{c_{0,0} - \lambda \ c_{0,\infty} + (c_{1,0} - \lambda \ c_{1,\infty})T + (\lambda - 1) \log(R)} \quad (15)$$

is used, which normalizes the raw DC-resistance values R using the current temperature T of the material. The parameters c and λ were fitted in advance.

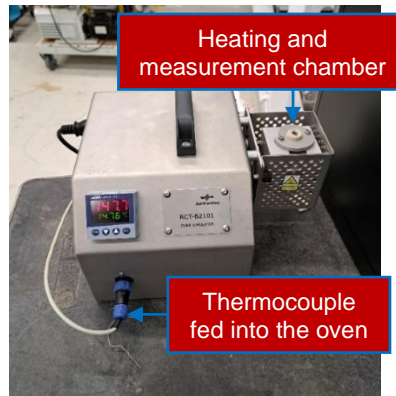


Fig. 5. External reference sensor

3. Results

For the verification of the developed approach, 12 experiments with different nominal process parameters were conducted (see Table 4). Naturally the actual temperature evolution in the oven lags the nominal temperature profile and depends on the controller.

Table 4. Overview of the nominal process parameters of the conducted experiments

Experiment No.	Heating Ramp	Isothermal Curing Temperature	Isothermal Curing Time
	K/min	°C	min
1	4	180	150
2	2,5	180	165
3	2,5	180	165
4	2,5	175	180
5	3	180	150
6	3	180	165
7	3	180	180
8	2,5	180	180
9	3	175	120
10	3	175	150
11	3,25	185	120
12	3	175	165

A short sequence of the DA-process is shown in Fig. 6 for a surface node in the center of the sample. Every mean prediction (yellow curve) is compensated by the infrared image data (green curve) which results in a new state (blue curve), which is the ensembles mean. It should be noted that the measurement data \hat{y}_k is not directly comparable with the state

data x_k due to Eq. (14). The measurement data, if converted to actual temperature data using the inverse of Eq. (14), would be below the ensembles mean state since it is a combination of prediction and measurement, i.e. a linear shift between them.

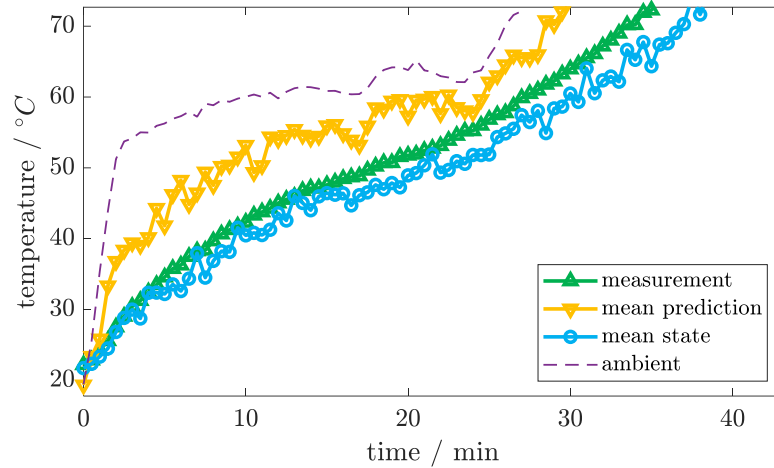


Fig. 6. Example of the DA process.

The thermal data of one experiment is depicted in the left graph of Fig. 7. Depending on the sensor position the thermal lags are different. The ambient temperature shows the fastest rise, followed by the tool surface temperature. The core temperature of the sample (where the reference thermocouple is placed) rises the slowest. The according differences of each sensor to this reference are shown in the right graph of Fig. 7.

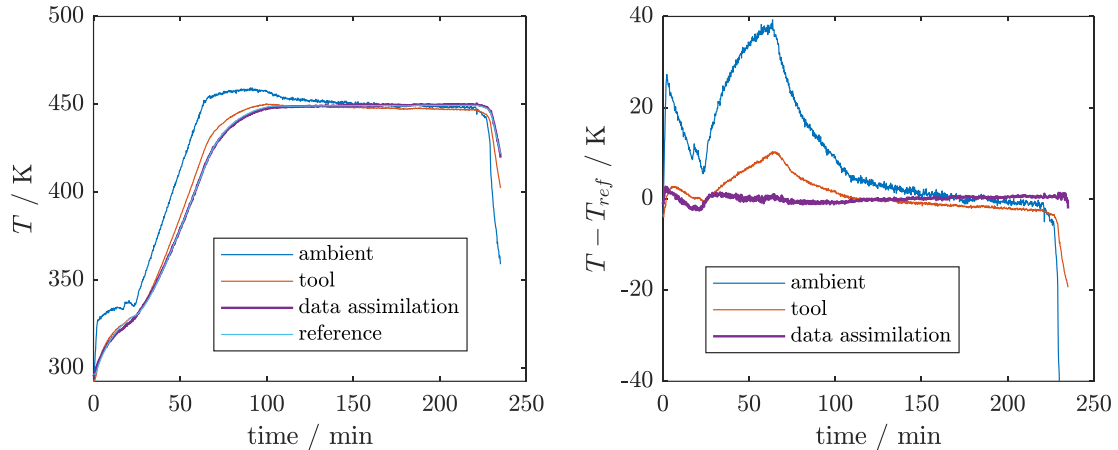


Fig. 7. Temperature (left) and the thermal lag with respect to the thermocouple of the reference sensor (right).

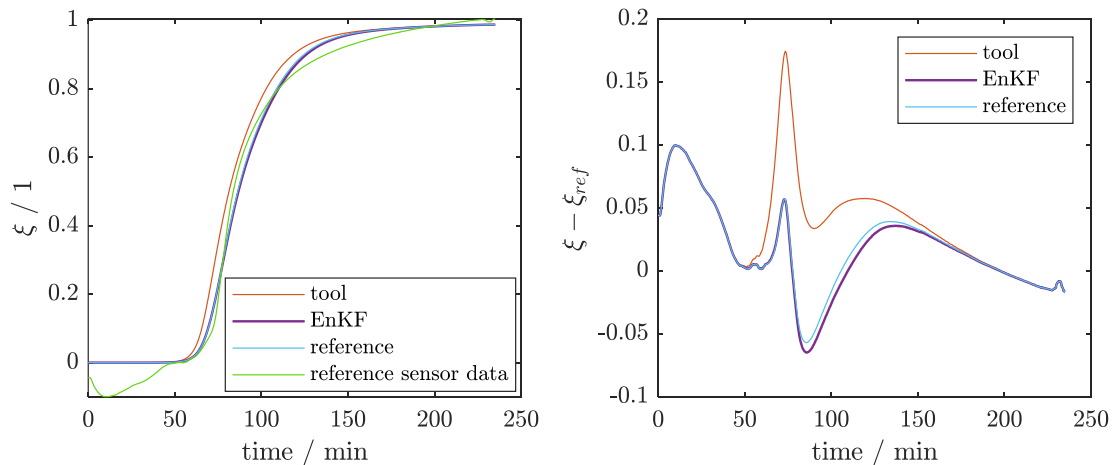


Fig. 8. Degree of Cure (left) and according differences of the DoC with respect to the reference sensor data (right).

The EnKF-based measurement method follows closely the reference sensor. With respect to the estimation of the core temperature of the part, this indicates the improved accuracy of the IR-based monitoring system compared to the tool temperature. The solution of Eq. (11)-(13) using these temperature data of Fig. 7 is shown in the left graph of Fig. 8. Using the tool temperature a significant deviation to the actual DoC of the center of the sample is evident, especially in early stages of the curing. Again the EnKF-based approach shows improved results. However deviations to the reference sensor data are present which is likely due to the difference in the physical properties, which are underlying the reference sensor and the EnKF-approach. While the former measures the DC-resistance respectively the ion viscosity, the latter is based on the heat of reaction respectively on the thermo-chemical behaviour. Furthermore, phenomena like resin flow towards the measuring surface are present at the beginning of the curing process, which causes the reference sensor to exhibit strong artifacts in these stages.

For each of the conducted experiments mean absolute errors (MAE) to the reference sensor were calculated. Median values of the MAEs are shown in Table 5 for the temperature estimation and for the DoC estimation.

Table 5. MAE (median values over 12 experiments) to reference point (core of sample)

	Temperature / K	DoC / %
Tool temperature with OD cure kinetics	2.60	3.43
Infrared measurement with data assimilation	1.35	3.03

4. Discussion

The material behaviour during the curing process and the underlying chemical and physical phenomena provides important information that enables the efficient curing of reactive resins. In general, monitoring the curing process involves the analysis of material properties during curing. Besides measuring electrical, optical, mechanical, chemical, or acoustic properties, the characterisation of the curing process based on thermophysical properties is possible. Although there are many different techniques for the thermophysical characterisation of the curing process, they can only be applied ex-situ, i.e. under laboratory conditions, and generally cannot be applied in-situ during an industrial curing cycle. Usually, ex-situ methods require the destruction of the material and may not sufficiently or only partially replicate the true environmental conditions. These methods necessitate the capture of the entire thermal cycle to ensure comparability. Typically, a min-max normalization technique is applied for this purpose. The presented approach has the clear advantage that real thermal data can be used to estimate the degree of cure in-situ and in real time.

Compared to the reference sensor there are also distinct advantages, since in real applications the thermocouple of the reference sensor would be placed in close vicinity to the part and not inside. This would lead to a considerable thermal lag between the actual part temperature and the temperature used for the reference sensor, especially in thick composites. Furthermore, the exothermal reaction inside the part is not measured when the thermocouple is not inside the part. This leads to inaccurate thermal data that is used for the sensor and an additional time reserve must be considered to ensure that the part is also properly cured inside.

While the developed approach allows an improved temperature estimation, the improvement in the DoC estimation is less significant. However for thicker and complex shaped composites, the accuracy improvement becomes more significant. The application of the developed approach to complex parts is possible since the dynamic prediction model can be adapted easily. The presented method could be extended and improved in several ways. For example, a combined state and parameter estimation, by augmenting the state vector with material and model parameters, could increase the model accuracy. By extending the model with a dielectric model, the reference sensor can be integrated in the monitoring system. In general an arbitrary number of sensors (like additional cameras or thermocouples) can be integrated.

5. Acknowledgement

The financial support by the Austrian Research Funding Association (FFG), within the project "Zero Defect Manufacturing for Thermo-dynamical Processes" (Contract No. #883864), is gratefully acknowledged.

REFERENCES

1. Menczel JD, Prime RB (eds) (2009) Thermal analysis of polymers. John Wiley, Hoboken, N.J
2. Ma W, Jafarpour B, Qin J (2019) Dynamic characterization of geologic CO₂ storage aquifers from monitoring data with ensemble Kalman filter. International Journal of Greenhouse Gas Control 81:199–215. <https://doi.org/10.1016/j.ijggc.2018.10.009>
3. Evensen (2022) Data Assimilation Fundamentals. Springer International Publishing
4. Evensen G (1994) Sequential data assimilation with a nonlinear quasi-geostrophic model using Monte Carlo methods to forecast error statistics. J Geophys Res 99:10143–10162. <https://doi.org/10.1029/94JC00572>
5. Katzfuss M, Stroud JR, Wikle CK (2016) Understanding the Ensemble Kalman Filter. The American Statistician 70:350–357. <https://doi.org/10.1080/00031305.2016.1141709>

6. Evensen G (2009) The ensemble Kalman filter for combined state and parameter estimation. *IEEE Control Syst* 29:83–104. <https://doi.org/10.1109/MCS.2009.932223>
7. Evensen G (2003) The Ensemble Kalman Filter: theoretical formulation and practical implementation. *Ocean Dynamics* 53:343–367. <https://doi.org/10.1007/s10236-003-0036-9>
8. Roth M, Hendeby G, Fritsche C et al. (2017) The Ensemble Kalman filter: a signal processing perspective. *EURASIP J Adv Signal Process* 2017. <https://doi.org/10.1186/s13634-017-0492-x>
9. Ishizuka J, Matsuzaki R, Tachikawa T (2019) Data assimilation-based state estimation of composites during molding. *Advanced Composite Materials* 28:225–243. <https://doi.org/10.1080/09243046.2018.1482513>
10. Oka Y, Ohno M (2020) Parameter estimation for heat transfer analysis during casting processes based on ensemble Kalman filter. *International Journal of Heat and Mass Transfer* 149:119232. <https://doi.org/10.1016/j.ijheatmasstransfer.2019.119232>
11. Yokoyama R, Matsuzaki R, Kobara T et al. (2020) Sequential estimation of the generated curing heat of composite materials by data assimilation: A numerical study. *Heliyon* 6:e05147. <https://doi.org/10.1016/j.heliyon.2020.e05147>
12. Chen C, Li Y, Gu Y et al. (2018) An improved simplified approach for curing kinetics of epoxy resins by nonisothermal differential scanning calorimetry. *High Performance Polymers* 30:303–311. <https://doi.org/10.1177/0954008317693291>
13. Pantelelis N, Bistekos E, Gerrits W et al. (2021) Non-intrusive Online Tg for the efficient manufacturing of CFRP. In: *Proceedings of the SAMPE 2021 Conference*
14. Pascault JP, Williams RJJ (1990) Glass transition temperature versus conversion relationships for thermosetting polymers. *J Polym Sci B Polym Phys* 28:85–95. <https://doi.org/10.1002/polb.1990.090280107>